Supporting Information

Identification of Oxidized Platinum Single Atoms on Chlorinated γ–Alumina Support by Density Functional Theory Calculations and X-Ray Absorption Spectroscopy

Adrien Hellier,[1] Ana T. F. Batista,[1] Christèle Legens,[1] Antonio Aguilar Tapia,[2,#] Olivier Proux,[3] Jean-Louis Hazemann,[2] Anne-Sophie Gay,[1] Yves Joly,[2] Céline Chizallet,[1] Pascal Raybaud[1,4,*]

[1] IFP Energies nouvelles, Rond-point de l'échangeur de Solaize, BP3, 69360 Solaize, France

[2] Institut Néel, UPR 2940 CNRS Université Grenoble Alpes, F-38000 Grenoble, France

[3] OSUG, UAR 832 CNRS-Université Grenoble Alpes, F-38041 Grenoble, France

[4] Univ Lyon, ENS de Lyon, CNRS, Université Claude Bernard Lyon 1, Laboratoire de Chimie UMR 5182, F-69342 Lyon France

#current address: Institut de Chimie Moléculaire de Grenoble, UAR2607 CNRS Université Grenoble Alpes, Grenoble F-38000, France

*Corresponding author: pascal.raybaud@ifpen.fr

SI 1. EXAFS spectra of the Pt powder and PtO_2 references.

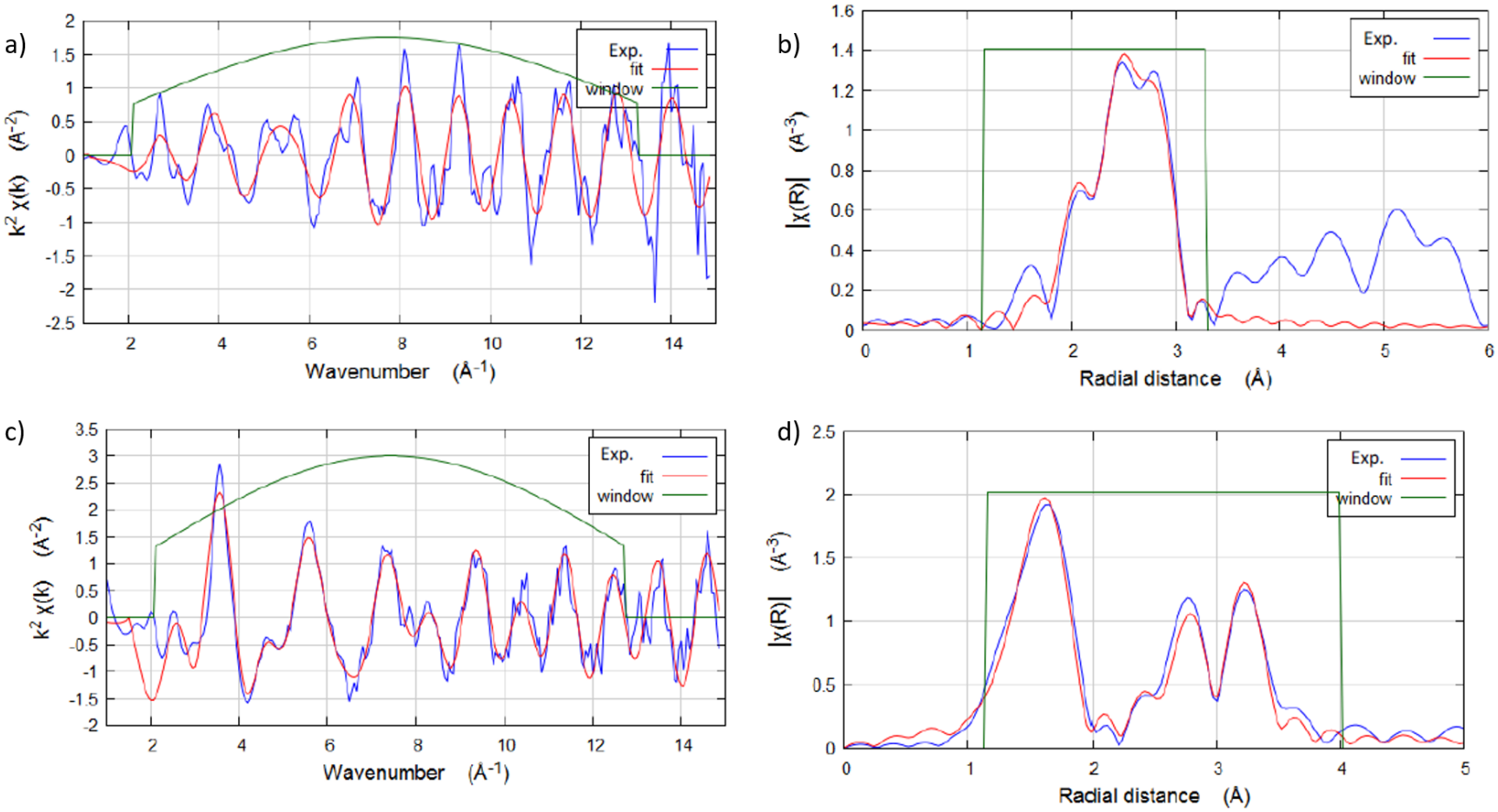

Figure S1. EXAFS and magnitude of the Fourier Transform weighted by k^2 of the references Pt powder (a, b) and PtO_2 (c, d).

	Path origin*	Path	Coordination number**	R (Å)	σ^2 (Å^2)	S_0^2	ΔE_0	R-factor	N_{ind}	N_{par}
PtO_2 (2017)	PtO_2 (1530633)	P-O (1)	6	2.013±0.006	0.002±0.002	0.89±0.04	9.93±0.76	0.02	18	10
	PtO_2 (1537410)	Pt-Pt	6	3.102±0.006	0.002±0.001					
		Pt-O (2)	6	3.66±0.03	0.004±0.006					
		Pt-O (3)	6	4.04±0.04	0.01±0.01					
PtO_2 (2018)	PtO_2 (1530633)	P-O (1)	6	2.009±0.008	0.003±0.002	0.86±0.05	8.65±0.94	0.02	18	12
	PtO_2 (1537410)	Pt-Pt	6	3.100±0.010	0.002±0.001					
		Pt-O (2)	6	3.67±0.05	0.003±0.007					
		Pt-O (3)	6	3.6±0.1	0.01±0.02					
		Pt-O (4)	6	4.05±0.08	0.02±0.02					

Table S1. EXAFS fitting of reference corresponding to the red line on the figure above. *Crystallographic structure ID in parenthesis; **Coordination number is fixed

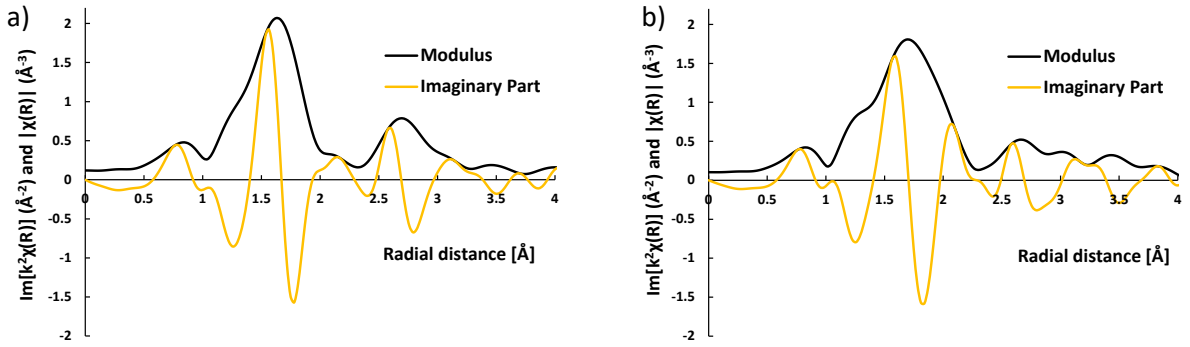

Figure S2. EXAFS results for 0.3 wt.% Pt supported on γ-Al_2O_3 at a) 0.1 wt.% Cl and b) 1.4 wt.% Cl. k^2 weighted Fourier transform modulus |χ(R)| (no phase correction) and imaginary part.

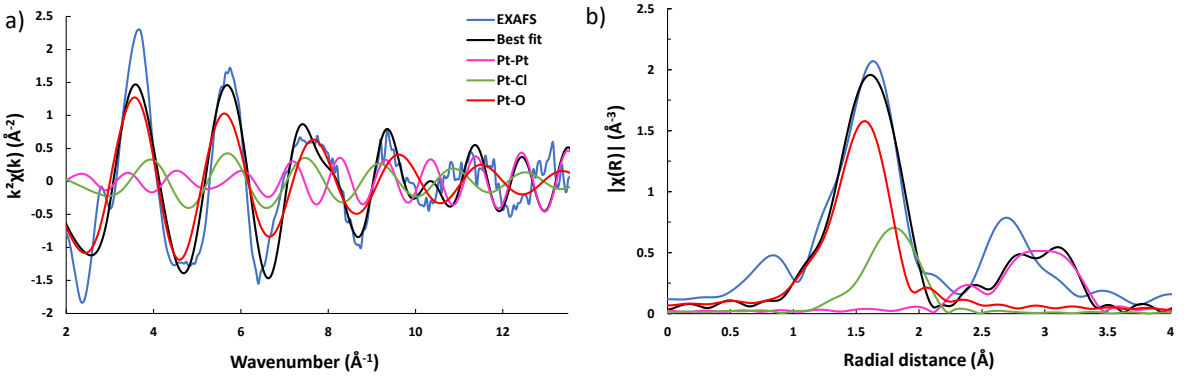

Figure S3. EXAFS results for 0.3 wt.% Pt supported on γ-Al_2O_3 at 0.1 wt.% Cl: a) EXAFS k^2χ(k) oscillations (blue), b) magnitude of the Fourier transform |χ(R)| (blue, without phase correction). The black lines represent the best fit (with R factor of 0.09) using Pt in the second shell initiated from Pt-Pt path (pink line) found in PtO_2 reference phase (1537410, see Table S1). The green and red lines represent the Pt-O, Pt-Cl neighbors' paths initiated from $PtCl_4$ (Pearson 1214146) and PtO_2 (1537410).

SI 2. DFT model of the (100) γ–alumina surface

We considered a 2x3 supercells with respect to the Digne's unit cell[1] (**Figure S4**). The slab considered is made of four alumina layers and the first two layers were relaxed during geometry optimizations.

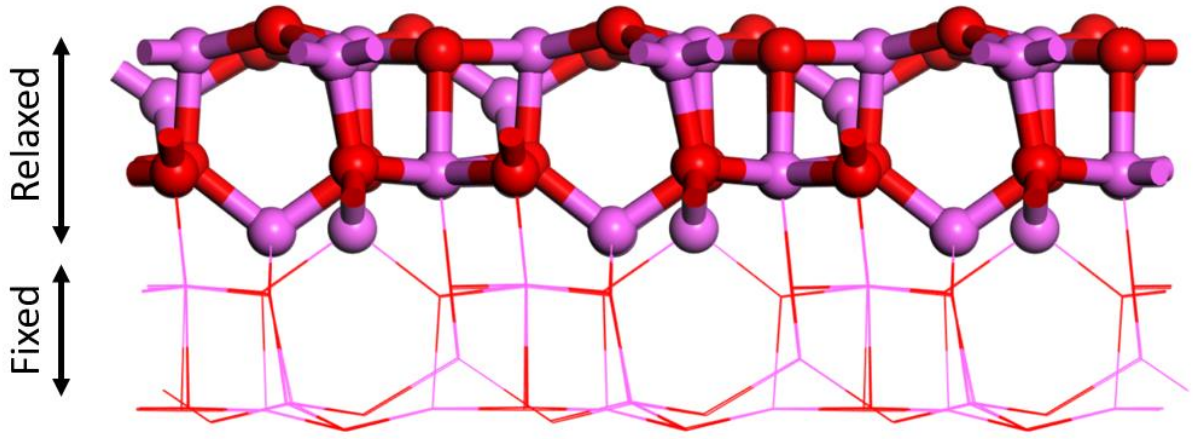

Figure S4. Side view of the molecular model of the (100) surface of γ-Al_2O_3. Color code for atomic structures: O: red; Al: pink.

SI 3. FDMNES simulation of Pt_{bulk} XANES

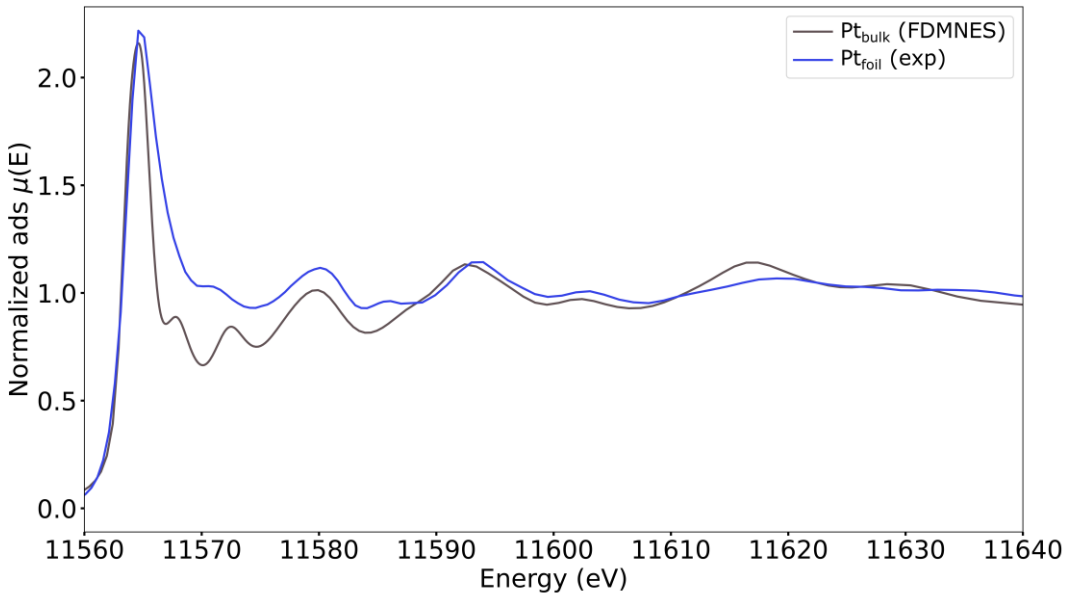

Figure S5. Pt L_3-edge calculation compared to the Pt L_3-edge of the Pt_{foil} reference.

SI 4. Scanning transmission electron microscopy.

High resolution high angle annular dark field in scanning transmission electron microscopy (HR-HAADF-STEM) imaging was carried out on a Cs-corrected JEOL JEM 2100F microscope accessible at , operated at 200 kV, equipped with a JEOL HAADF detector. For the HR-STEM images, the camera length used in the HAADF mode was 10 cm, corresponding to inner and outer diameters of the annular detector of 60 and 160 mrad, respectively. The size of the electron probe in STEM mode is 0.11 nm. Before the STEM analyses, the powdered samples were deposited without solvent on a 300 mesh holey carbon copper grid.

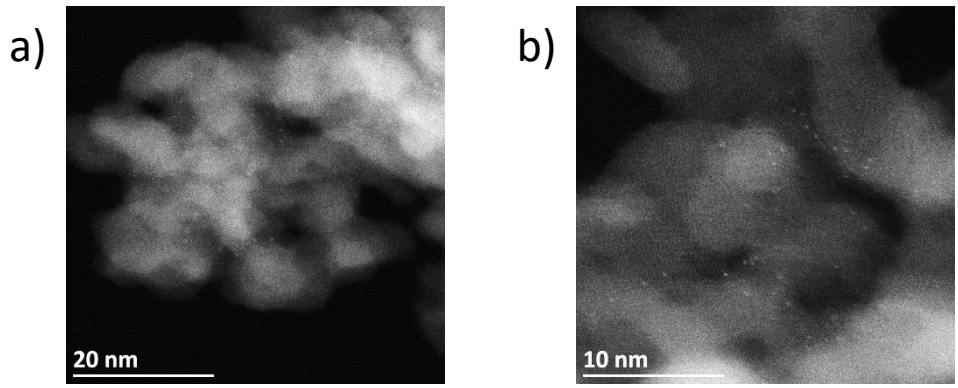

Figure S6. HR-HAADF-STEM images of Pt oxychloride supported on γ-alumina (0.3 wt.% Pt over PuralSB3 with 1.4 wt.% Cl).

SI 5. Structural and electronic properties of the various simulated Pt complexes.

Stoichiometry	d(Pt-O_{surf}) (Å)	d(Pt-Cl) (Å)	d(Pt-OH) (Å)	d(Pt-O) (Å)	d(Pt-OH_2) (Å)	Pt charge (e)	Ligands charge (e)	Surface charge (e)	Grafting site
PtO_2	2.07 2.15			1.79 1.94		0.580	-0.656	0.075	O_A-O_C
$PtOCl_2$	2.08	2.24 2.26		1.86		0.490	-0489	0.002	O_B
PtOCl(OH)	2.05	2.24	1.96	1.85		0.543	-0.515	-0.026	O_B
$PtO(OH)_2$	2.05		1.91 1.98	1.84		0.604	-0.458	-0.148	O_B
$PtCl_4$	2.11	2.26 2.28 2.29 2.32				0.498	-0.285	-0.216	O_B
$PtCl_3(OH)$	2.00	2.23 2.28 2.34	2.05			0.543	-0.488	-0.05	O_B
$PtCl_2(OH)_2$	2.04	2.27 2.27	2.01 2.04			0.621	-0.387	-0.234	O_B
$PtCl(OH)_3$	1.98	2.23	2.00 2.04 2.04			0.637	-0.372	-0.266	O_B
$Pt(OH)_4$	1.97		1.90 2.00 2.03 2.05			0.684	-0.355	-0.331	O_B
$PtCl_4(OH)H$*	2.11	1.90 2.00 2.03 2.05	2.07			0.493	-0.466	-0.039	O_B
$PtCl_3(OH)_2H$*	2.09	2.28 2.29 2.30	2.05 2.06			0.537	-0.508	-0.035	O_B
$PtCl_2(OH)_2(H_2O)$	2.05	2.29 2.30	2.01 2.04		2.05	0.597	-0.368	-0.228	O_B
$PtCl(OH)_3(H_2O)$	2.02	2.30	2.00 2.01 2.03		2.05	0.643	-0.356	-0.283	O_B
$Pt(OH)_4(H_2O)$	2.04	1.99 2.00 2.02 2.03			2.05	0.683	-0.382	-0.299	O_B

Table S2. Geometric description and platinum charge of supported complexes. Ligands charge is the sum of the Hirshfeld charges of all ligands (except surface atoms). Surface charge is the sum of all the Hirshfeld charges of aluminium and oxygen of the surface. Grafting site refers to the nature of the oxygens of the alumina support bonded to the Pt. The choice was made to keep for a given stoichiometry only the most stable isomer. Due to the acidic nature of the Al_2O_3 surface, protons could also be adsorbed on the surface oxygen atoms to form surface hydroxyls. A star (*) will be used to differentiate these structures.

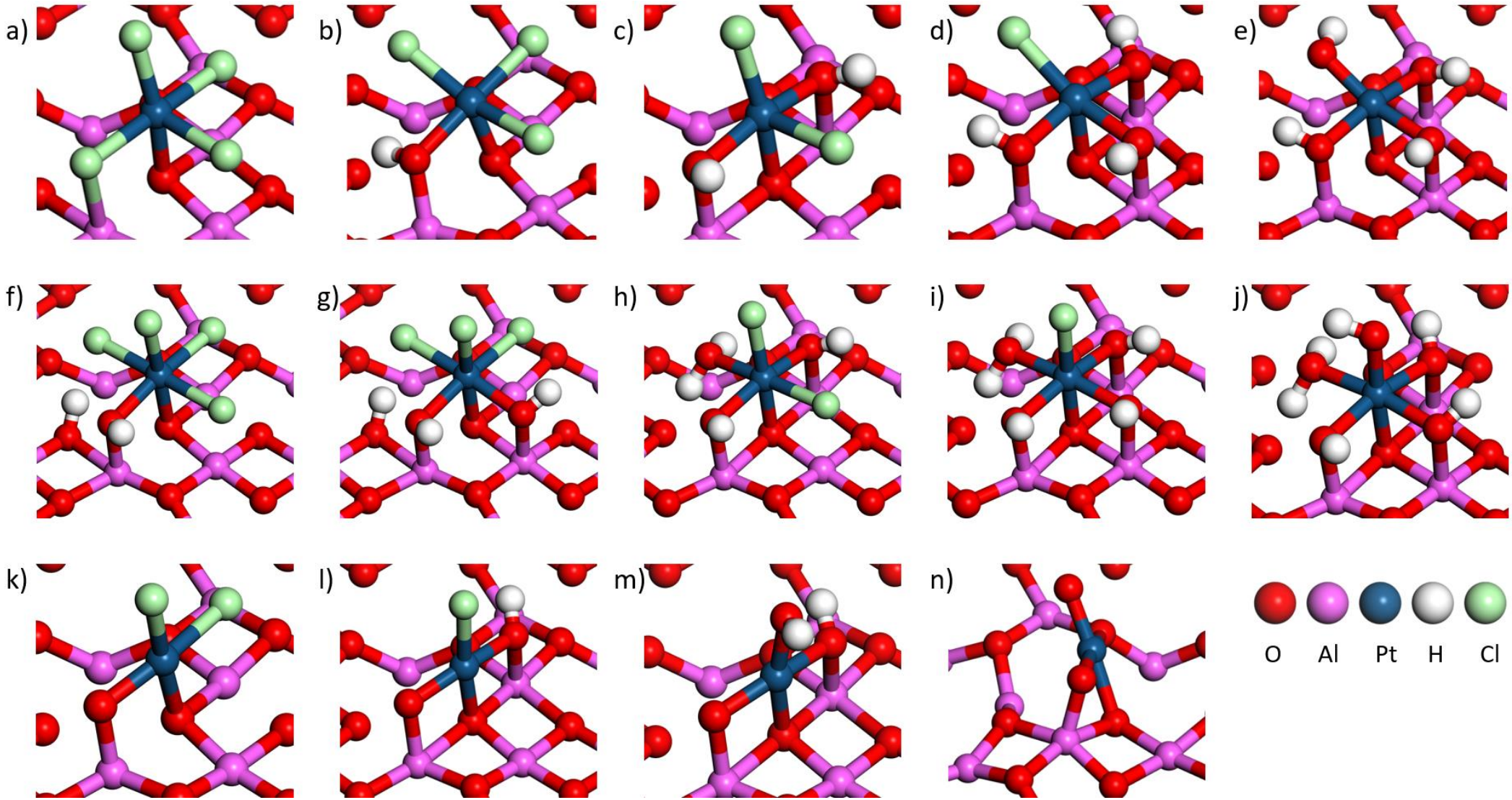

Figure S7. Optimized structures of supported Pt(IV) complexes considered to model the calcination step. a) $PtCl_4$, b) $PtCl_3(OH)$, c) $PtCl_2(OH)_2$, d) $PtCl(OH)_3$, e) $Pt(OH)_4$, f) $PtCl_4(OH)H$*, g) $PtCl_3(OH)_2H$*, h) $PtCl_2(OH)_2(H_2O)$, i) $PtCl(OH)_3(H_2O)$, j) $Pt(OH)_4(H_2O)$, k) $PtOCl_2$, l) $PtOCl(OH)$, m) $PtO(OH)_2$, n) PtO_2. The cif files of these structures are accessible upon request or in the compressed file accessible online.

SI 6. Energetics

During the calcination process, changes on the coordination sphere of the platinum species are expected. As explained in the methods (**Eq.1-Eq4**), we will consider that such changes occur through hydration reactions (blue arrows in **Figure 1** of the main text) and ligand exchange (combination of 1 blue and 1 red arrow in **Figure 1**). In this part, we describe the energetics of these reactions at 0 K to provide a better understanding of the final surface thermochemical trend.

Hydration reactions are always exothermic at 0 K and the average hydration energy is -156 kJ mol^{-1} (**Table S3**). The exothermicity is impacted by different factor such as the coordination sphere, the geometry, or the grafting mode of the complexes. In the absence of oxo ligand, hydrations are easier in presence of chlorine with hydration energies of -196 kJ.$mol^{-1}$for $PtCl_4$, -188.4 kJ mol^{-1} for $PtCl(OH)_3$ and -144.7 kJ mol^{-1} for $Pt(OH)_4$. No notable difference between the reaction energies described by **Eq.2** and **Eq.3** (undissociated water molecule, and formation of a surface hydroxyl) has been noticed. Interestingly, the trend is reversed in presence of oxo ligand (**Eq.4**) and hydration becomes harder with the number of chlorines in the coordination sphere of the platinum. In these cases, chlorine hardens the hydration by around 20 kJ mol^{-1}. The hydration of $PtOCl_2$ and PtOCl(OH) (into $PtCl_2(OH)_2$ and $PtCl(OH)_3$) are calculated at -108.4 kJ mol^{-1} and -126.9 kJ mol^{-1} respectively while the hydration of $PtO(OH)_2$ into $Pt(OH)_4$ is at -145.6 kJ mol^{-1}. The geometries of the hydrated complexes are also an important factor. In particular, the formation of octahedral complexes (from penta-coordinated ones) results in highly exothermic hydration reactions, between -144.7 kJ mol^{-1} and -196.0 kJ mol^{-1} for the hydration of $PtCl_y(OH)_z$. The grafting of the complexes can also modulate the hydration energies: PtO_2 is less hydrophilic than other complexes with only -106.6 kJ mol^{-1} calculated for its hydration into $PtO(OH)_2$. As in this case, the reactant and product exhibit a square planar geometry, the grafting mode rather than the geometry is suspected to be responsible for this

high stabilisation of PtO_2, probably due, to the high interaction energies (**Figure S8**) of the bi-grafted complex.

	ΔE (kJ/mol)
Hydration	
$PtCl_4 + H_2O \rightarrow PtCl_4(OH)H^*$	-196.0
$PtCl_3(OH) + H_2O \rightarrow PtCl_3(OH)_2H^*$	-193.1
$PtCl_2(OH)_2 + H_2O \rightarrow PtCl_2(OH)_2(H_2O)$	-194.3
$PtCl(OH)_3 + H_2O \rightarrow PtCl(OH)_3(H_2O)$	-188.4
$Pt(OH)_4 + H_2O \rightarrow Pt(OH)_4(H_2O)$	-144.7
$PtOCl_2 + H_2O \rightarrow PtCl_2(OH)_2$	-108.4
$PtOCl(OH) + H_2O \rightarrow PtCl(OH)_3$	-126.9
$PtO(OH)_2 + H_2O \rightarrow Pt(OH)_4$	-145.6
$PtO_2 + H_2O \rightarrow PtO(OH)_2$	-106.6
MAV	**-156.0**

Table S3. Reaction energies calculated at 0 K for hydration reactions relevant for calcination.

We notice that the support favors the Pt complex hydration with an overall gain of -85 kJ mol^{-1} compared to values calculated for similar reactions in gas phase (average reaction energies of -71 kJ mol^{-1} at PBE-dDsC level).[2] However, other factors have to be considered. Indeed, the geometry of the complex being an important factor of (de)stabilisation, it is not straightforward to compare the $PtCl_y(OH)_{4-y}$ complexes either supported or in gas phase, as they evolve from an unstable pentahedral geometries to stable octahedral ones (if supported), while in gas phase the homologous stable square planar are transformed into unstable pentahedral species. The mean hydration energies of the gas phase square planar $PtCl_y(OH)_{4-y}$ into pentahedral $PtCl_y(OH)_{4-y}(H_2O)$ and then octahedral $PtCl_y(OH)_{4-y}(H_2O)_2$ were calculated at -27.2 kJ mol^{-1} and -96.5 kJ mol^{-1}[2] while once supported, the mean hydration of the $PtCl_y(OH)_{4-y}$ is 183.3 kJ mol^{-1}. In a similar spirit, the comparison of the hydration of $PtOCl_y(OH)_{2-y}$ also supports the stabilizing impact of the support. Indeed, similar energies are calculated in gas phase where a square planar is formed (120.3 kJ mol^{-1}) and on the support where pentahedral complexes are formed (127.0 kJ mol^{-1}). In spite of these intricated effects, there is an undeniable role of the support in the stabilization of the hydrated $PtCl_y(OH)_{4-y}(H_2O)$ complexes. It may originate from

the interaction between the water ligand and the support either through chemical bonding (after its dissociation), or through hydrogen bonding or dispersion forces. Moreover, the Pt charge being more positive on the support, it acts as a stronger Lewis site for the basic O of the water molecules.

	ΔE (kJ/mol)
Ligand Exchange	
$PtCl_4 + H_2O \rightarrow PtCl_3(OH) + HCl$	14.1
$PtCl_3(OH) + H_2O \rightarrow PtCl_2(OH)_2 + HCl$	21.3
$PtCl_2(OH)_2 + H_2O \rightarrow PtCl(OH)_3 + HCl$	23.9
$PtCl(OH)_3 + H_2O \rightarrow Pt(OH)_4 + HCl$	46.1
$PtCl_4(OH)H^* + H_2O \rightarrow PtCl_3(OH)_2H^* + HCl$	17.0
$PtCl_3(OH)_2H^* + H_2O \rightarrow PtCl_2(OH)_2(H_2O) + HCl$	20.0
$PtCl_2(OH)_2(H_2O) + H_2O \rightarrow PtCl(OH)_3(H_2O) + HCl$	29.8
$PtCl(OH)_3(H_2O) + H_2O \rightarrow Pt(OH)_4(H_2O) + HCl$	89.9
$PtOCl_2 + H_2O \rightarrow PtOCl(OH) + HCl$	42.3
$PtOCl(OH) + H_2O \rightarrow PtO(OH)_2 + HCl$	64.9
MAV	**36.9**

Table S4. Reaction energies calculated at 0 K for ligand exchange reactions relevant for calcination.

Ligand exchange energies are calculated by considering the exchange of chlorine by hydroxyl (**Eq.1** and **Figure 1**). As shown by the positive reaction energies (average value of 36.9 kJ mol^{-1}), chlorinated species are intrinsically more stable than their hydroxylated counterpart (**Table S4**). A slightly more positive value was found for gas phase complexes, with an average energy of reaction of 53.2 kJ mol^{-1} for the same exchange reactions.[2] In a great number of cases, the hydroxyl formed upon H_2O/HCl exchange on the support becomes a bridging ligand between the Pt atom and one Al site (**Figure S7**) leading to stronger stability of the OH ligand (the interaction energy and its decomposition for each complex is detailed in **SI 7** and sum up in **Figure S8**), while the Cl bridging atom is less strongly bonded. This replacement of bonding ligands is possible up to 3 hydroxyls in the coordination sphere of the $PtCl_y(OH)_{4-y}(H_2O)_n$ complexes, which corresponds to the number of available aluminum sites around an oxygen B where the Pt complex is coordinated (**Figure S7**, **f-j**). The adsorption of $PtCl_y(OH)_{4-y}$ (**Eq.S4**) becomes stronger with the number of hydroxyls in the coordination sphere (**Figure S8**) and

reaches a plateau after 3 hydroxyls for $PtCl(OH)_3$ (-252.0 kJ mol^{-1}) and $Pt(OH)_4$ (-253.2 kJ mol^{-1}). A similar trend is found for the $PtCl_y(OH)_{4-y}(H_2O)$ octahedral complexes. However, in this case, the replacement of the last chlorine by an hydroxyl is calculated 19.9 kJ mol^{-1} higher on the support (+ 89.9 kJ mol^{-1} (**Table S3**) against 70 kJ mol^{-1} in gas phase[2]). In the presence of oxo ligands, the first exchange which allows the replacement of bridging chlorine into a bridging hydroxyl is also easier than in gas phase (+ 42.3 kJ mol^{-1} on the support and + 62 kJ mol^{-1} in gas phase[2]). During the last exchange, as the hydroxyl cannot interact with the support (exchanging it in place of the oxo ligand leads to an highly unstable conformer) the exchange is harder than in gas phase (64.9 kJ mol^{-1} (**Table S3**) against 49 kJ mol^{-1} in gas phase[2]). The fact that no exchange energy for the $PtCl_y(OH)_{4-y}$ pentahedral complexes exceeds the gas phase values even in the case of the 4^{th} hydroxyl is probably due to H-bonds between the last added hydroxyl and the support. Indeed, the distances between the hydrogen of the added hydroxyl and the two closest oxygens of the support are 3.09 Å and 3.39 Å, allowing the existence of H-bonds **Figure S7, a-e)**. In the cases of octahedral and square planar complexes, the last hydroxyls are in apical position, therefore no stabilizing interaction with the support is possible. Thus, the support facilitates the replacement of chlorines by hydroxyls as long as these new hydroxyls can form Pt-O(H)-Al bridging bonds.

SI 7. Interaction Energies

Definition

Various quantities such as the interaction energy, adsorption energy, complex deformation energy and surface deformation energy were determined at 0 K (without zero-point energy correction). Interaction energy describes how strongly complexes interact with the support and were calculated according to **Eq.S1**. The complex deformation energy is the destabilization resulting of the adsorption of the complex, it was calculated according to **Eq.S2**. Similarly, the deformation of the surface was calculated according to **Eq.S3**. Finally, the adsorption energy which describes the adsorption of a complex on the support by accounting of the interaction energy but also of the deformations induced by the adsorption was calculated according to E**q.S4**.

$$E^{int} = E_{system} - E'_{complex} - E'_{surface} \quad \textbf{Eq.S1}$$

$$E^{def}_{complex} = E'_{complex} - E_{complex} \quad \textbf{Eq.S2}$$

$$E^{def}_{surface} = E'_{surface} - E_{surface} \quad \textbf{Eq.S3}$$

$$E^{ads} = E^{int} - E^{def}_{complex} - E^{def}_{system} = E_{system} - E_{complex} - E_{surface} \quad \textbf{Eq.S4}$$

with E_{system} being the energy of the system (adsorbed complex + support). $E'_{complex}$ is the energy of the complex in gas phase with the same geometry and spin state as in the absorbed state. $E_{complex}$ is the energy of the complex after geometry and spin state optimization in gas phase. Similarly, $E'_{surface}$ is the energy of the surface without the complex adsorbed and for the geometry optimized after adsorption and $E_{surface}$ is the energy of the naked optimized surface. The spin state of the surface was considered to be a singlet.

Deformation energy analysis

After the adsorption of the complexes, constraints from the interaction between ligands and the surface induce a destabilization of the complexes compared to their reference geometries in gas phase (**Figure S8**). Other than the two spurious deformation energies of the complexes which undergo a dissociation ($PtCl_4(OH)H$* and $PtCl_3(OH)_2H$*) (**Figure S7, f and g**), the complexes' deformation energies are comprised between 23.3 kJ/mol ($PtOCl_2$) and 234.1 kJ/mol (PtO_2). As

for the adsorption energies represented in **Figure 5**, the deformation of the complex is related to both the geometry of the complex and the nature of the ligand. After adsorption, the three square planar complexes ($PtOCl_2$, PtOCl(OH) and $PtO(OH)_2$) (**Figure S7, k-l**) are the among the less impacted, with small deformation energies increasing from 23.3 kJ/mol for two chlorines ($PtOCl_2$) to 79 kJ/mol for two hydroxyls ($PtO(OH)_2$). This increase of the deformation energy with the exchange of chlorine by hydroxyl is well respected for these three complexes as they share similar geometries before and after adsorption. Indeed, the same trend is observed (after adsorption) for the three octahedral $PtCl_y(OH)_{4-y,\ y<3}(H_2O)$ (**Figure S7, h-j**) (75 kJ/mol for $PtCl_2(OH)_2(H_2O)$, 87 kJ/mol for $PtCl(OH)_3(H_2O)$ and 122 kJ/mol for $Pt(OH)_4(H_2O)$). Again, for these complexes, their adsorbed geometries are unique because of the five ligands already in the coordination sphere. However, the case of the pentahedral $PtCl_y(OH)_{4-y}$ is less straightforward as different geometries and changes from the gas phase reference are observed. (**Figure S7, a-e**) The deformation energies obtained are as follows: $PtCl_4$ with 69 kJ/mol; $PtCl_3(OH)$ with 85 kJ/mol; $PtCl(OH)_3$ with 89 kJ/mol $Pt(OH)_4$ with 110 kJ/mol and finally $PtCl_2(OH)_2$ with 136 kJ/mol. This last unexpectedly high deformation energy is related to the geometry of $PtCl_2(OH)_2$ after adsorption (**Figure S7-c**), which has a chlorine atom in an apical position while all of the other $PtCl_y(OH)_{4-y}$ are square planar in gas phase.[2] While all of them go from a square planar geometry to a pentahedral one, only $PtCl_4$ and $PtCl_2(OH)_2$ exhibit an apical ligand. The reason why $PtCl_4$ is less impacted despite its similar behaviour remains unclear. Perhaps this atypical ligand effect persists but is compensated by the fully chlorinated coordination sphere limiting further deformation.

In a similar way, the surface is also destabilized during the adsorption of the complexes (**Figure S8**). This quantity is mostly driven by the number of bridging ligands, their nature and the adsorption site. As for the deformation of the complexes, chlorines tend to be less constraining for the surface than hydroxyls with again some subtilities coming from the geometries of the

complexes after adsorption. The relative impact of oxo ligand is hard to evaluate as it is only present on complexes with specific geometries limiting the analysis of trends. Indeed, oxo ligands are in PtO_2 which exhibits the highest surface deformation energy (+ 221 kJ/mol) and is the only complex in the O(A)-O(C) adsorption site (**Figure S7, n)**). They are also present in the $PtOCl_y(OH)_{2-y}$ series which are again the only complexes bonded to the support by two bridging ligands. However, this low number of bonds with the surface allows small deformation of the surface with only 79 kJ/mol for $PtOCl_2$, 87 kJ/mol for PtOCl(OH) and 85 kJ/mol for $PtO(OH)_2$. As the oxo ligand is always bridging, both PtOCl(OH) and $PtO(OH)_2$ (**Figure S7**, **l and m)**) have the same bridging ligands, explaining their similar impact on the surface. Beside these four complexes, all the remaining ($PtCl_y(OH)_{4-y}$ and $PtCl_y(OH)_{4-y}(H_2O)$) are bonded to the surface by one Pt-O bond and three Pt-X-Al (X being a ligand) and the relative impact of Cl and OH is, quite, well-illustrated. The less constraining complex to the surface (77 kJ/mol) is the $PtCl_4$ which is the only complex with three Pt-Cl-Al bonds, followed by $PtCl_2(OH)_2$ at 89 kJ/mol. Both $Pt(OH)_4$ and $PtCl(OH)_3$ share similar anchoring ligands (3 Pt-O(H)-Al) and thus they distorted the surface in similar proportion with 143 kJ/mol and 147 kJ/mol respectively. The surface is quite insensitive to the addition of a water molecule to these two complexes, with 141 kJ/mol for $PtCl(OH)_3(H_2O)$ and 151 kJ/mol for $Pt(OH)_4(H_2O)$. However, in the case of $PtCl_2(OH)_2(H_2O)$, despite sharing geometric similarities with the last two octahedral complexes, the addition of H_2O results in a stronger surface deformation (+120 kJ/mol) compared to the pentahedral $PtCl_2(OH)_2$. The formation of a surface hydroxyl for both $PtCl_4(OH)H^*$ and $PtCl_3(OH)_2H^*$ is responsible for a bigger impact on the surface with deformations calculated at 151 kJ/mol and 168 kJ/mol respectively. Unexpectedly and totally off the trends lies $PtCl_3(OH)$ (**Figure S7**, **b)**) with 174 kJ/mol. In this case, the presence of only one Pt-O(H)-Al bond is responsible for strong elongation of an Al-O bond of the surface that cannot be compensated by the presence of a symmetric Pt-O(H)-Al as in all other complexes.

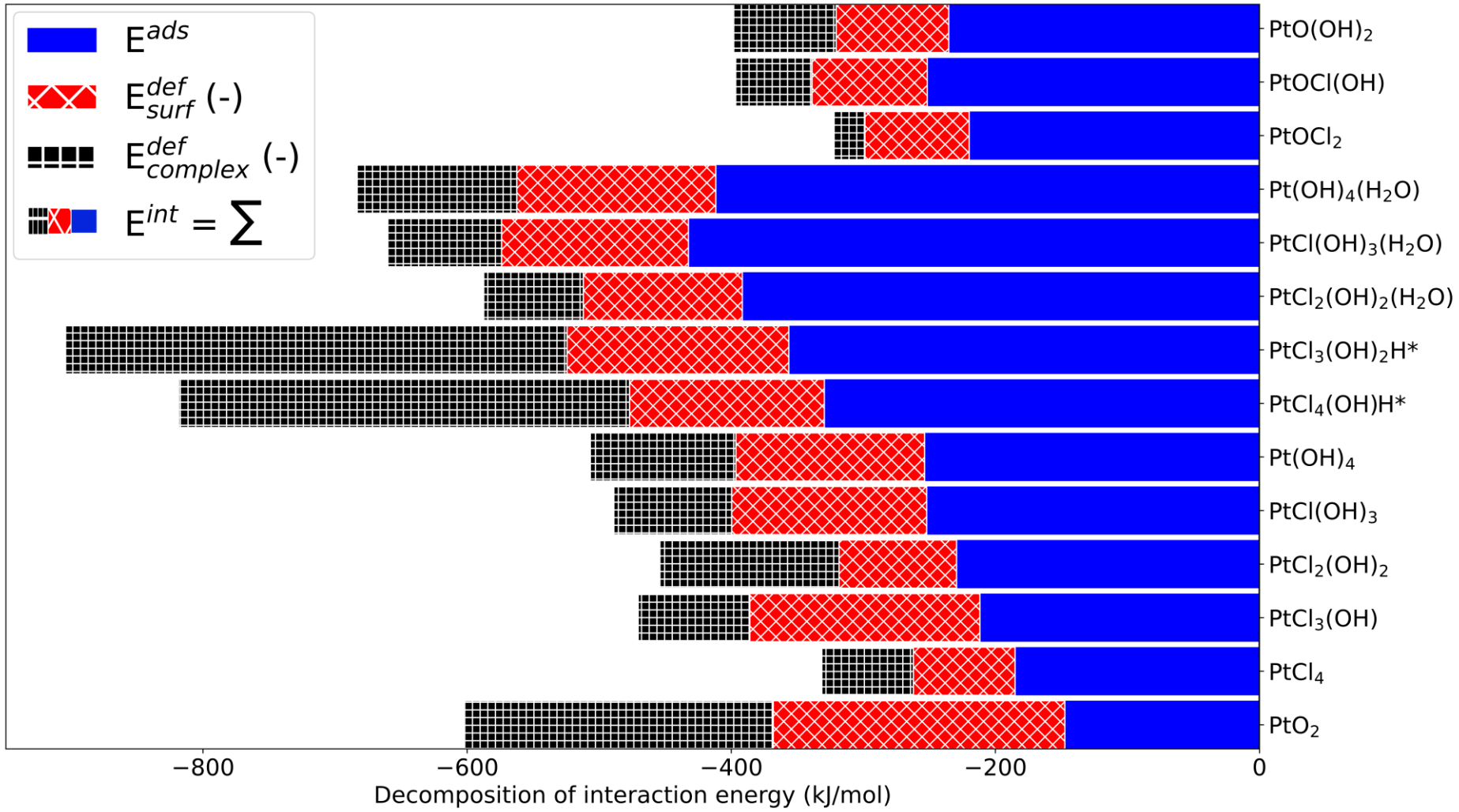

Figure S8. Decomposition of the interaction energy for supported complexes. Both deformations are reported as negative value for the sake of clarity. The interaction energy is the sum of the three quantities: $E^{ads} + E^{def}$ (surf) + E^{def}(complex) as described by Eq.S1-S3.

SI 8. Thermodynamic diagram for calcination. Impact of H_2O and HCl at fixed calcination temperature, calculated at the PBE-dDsC level.

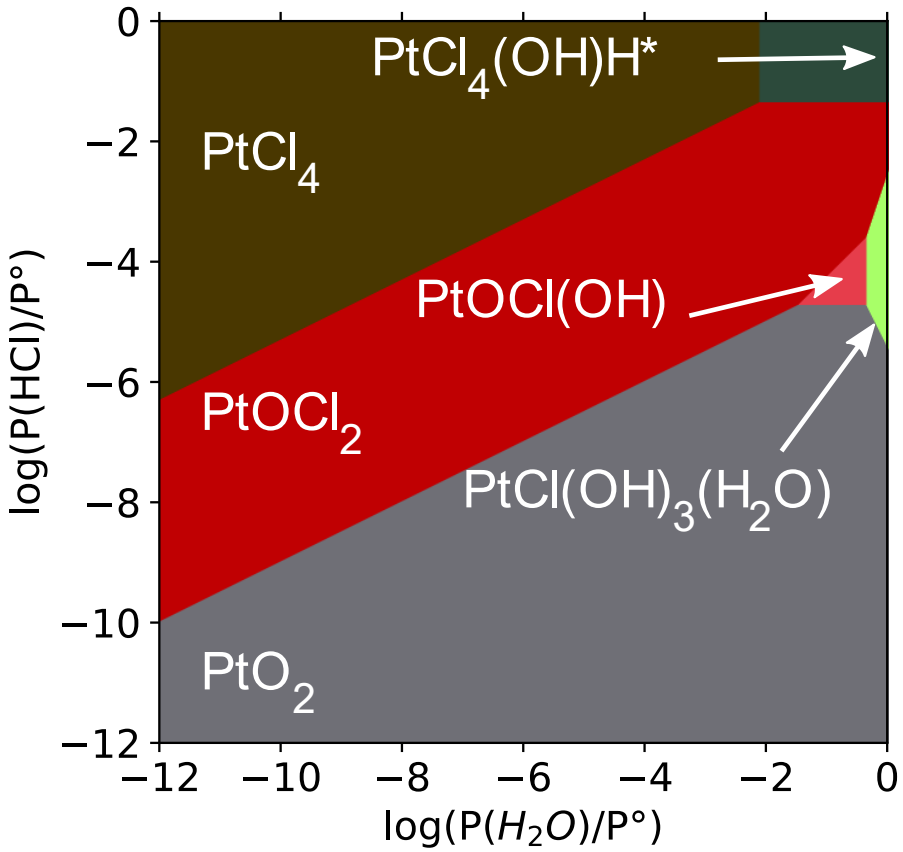

Figure S9. Thermodynamic diagrams of the most stable species under oxidative conditions at T = 800 K.

SI 9. Calcination and reduction thermodynamic diagrams calculated at the HSE06 level.

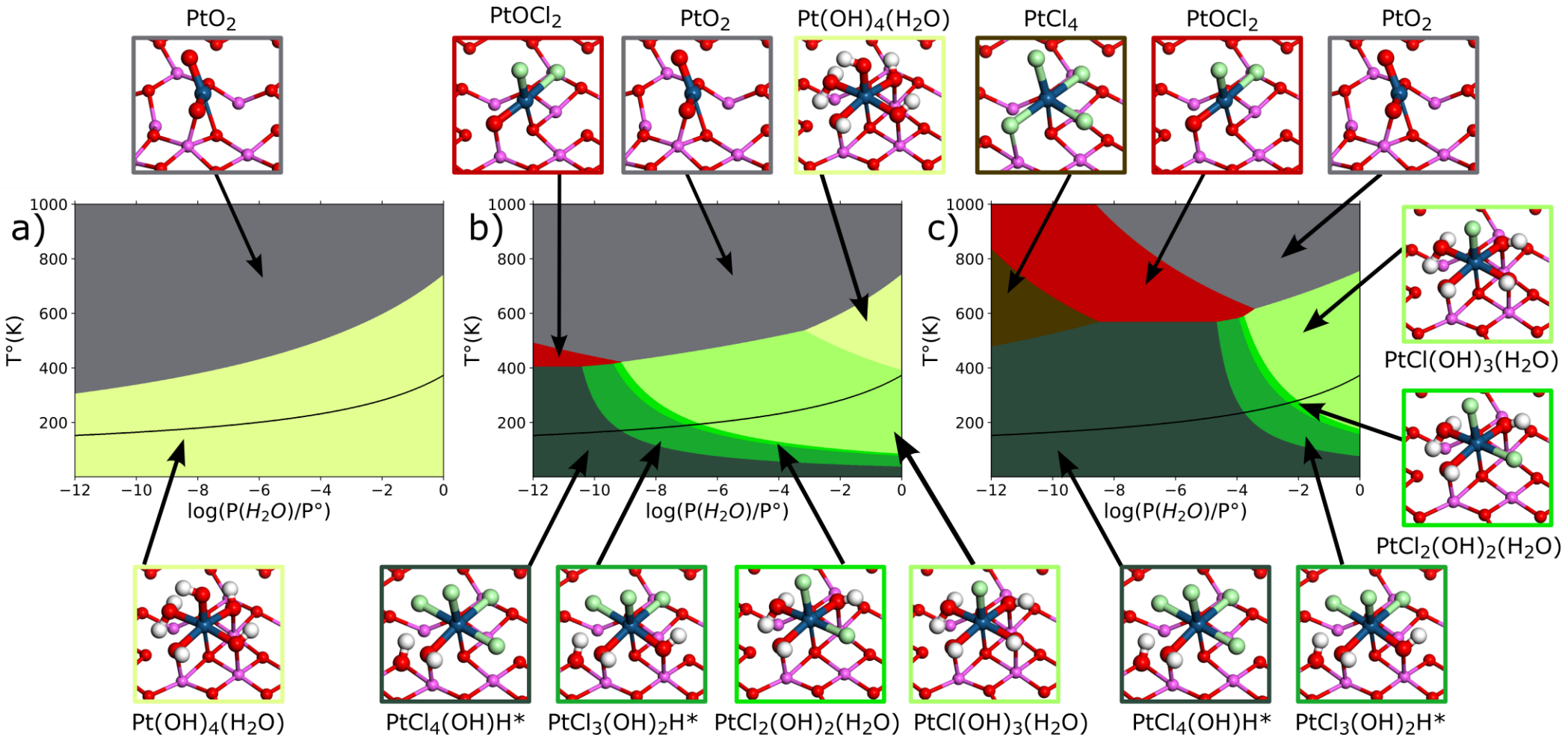

Figure S10. Thermodynamic diagrams calculated at the HSE06 level of the most stable species under oxidative conditions at $P(O_2)$ = 0.21 bar for three chlorine loadings: a) Without chlorine; b) P(HCl) = 1.10^{-12} bar; c) P(HCl) = 1.10^{-6} bar. The gas phase domain of water is located above the black curved line, representing the liquid/vapor equilibrium. Atoms' colors are blue for Platinum, red for oxygen, green for chlorine, pink for aluminum and white for hydrogen.

SI 10. DFT calculated Pt-Al and Pt-O_{long} distances in octahedral platinum complexes.

Pt complex	CN(Pt-Al)	Mean d(Pt-Al) (Å)	CN(Pt-O_{long})	Mean d(Pt-O_{long}) (Å)
$PtCl_4(OH)H$*	3	3.16	4	3.70
$PtCl_3(OH)_2H$*	3	3.10	4	3.64
$PtCl_2(OH)_2(H_2O)$	3	3.07	4	3.61
$PtCl(OH)_3(H_2O)$	3	3.00	4	3.56
$Pt(OH)_4(H_2O)$	3	2.99	4	3.55

Table S3. Averaged second shell distances and coordination number (CN) for the octahedral $PtCl_y(OH)_{4-y}(H_2O)$ species

SI 11. FEFF simulation of DFT models of octahedral $PtCl_y(OH)(H_2O)$ supported on the γ-alumina surface

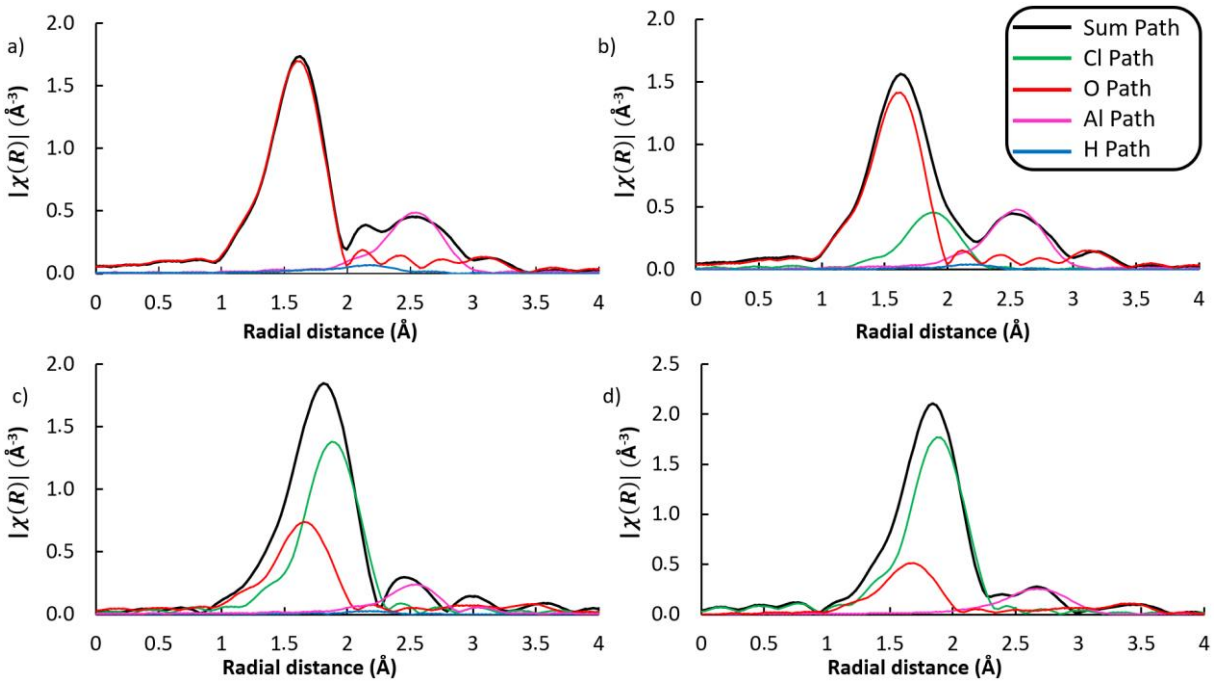

Figure S11. FEFF simulation of the k²-weighted magnitude of the Fourier transform (FT). a) $Pt(OH)_4(H_2O)$, b) $PtCl(OH)_3(H_2O)$, c) $PtCl_3(OH)_2H^*$, d) $PtCl_4(OH)H^*$.

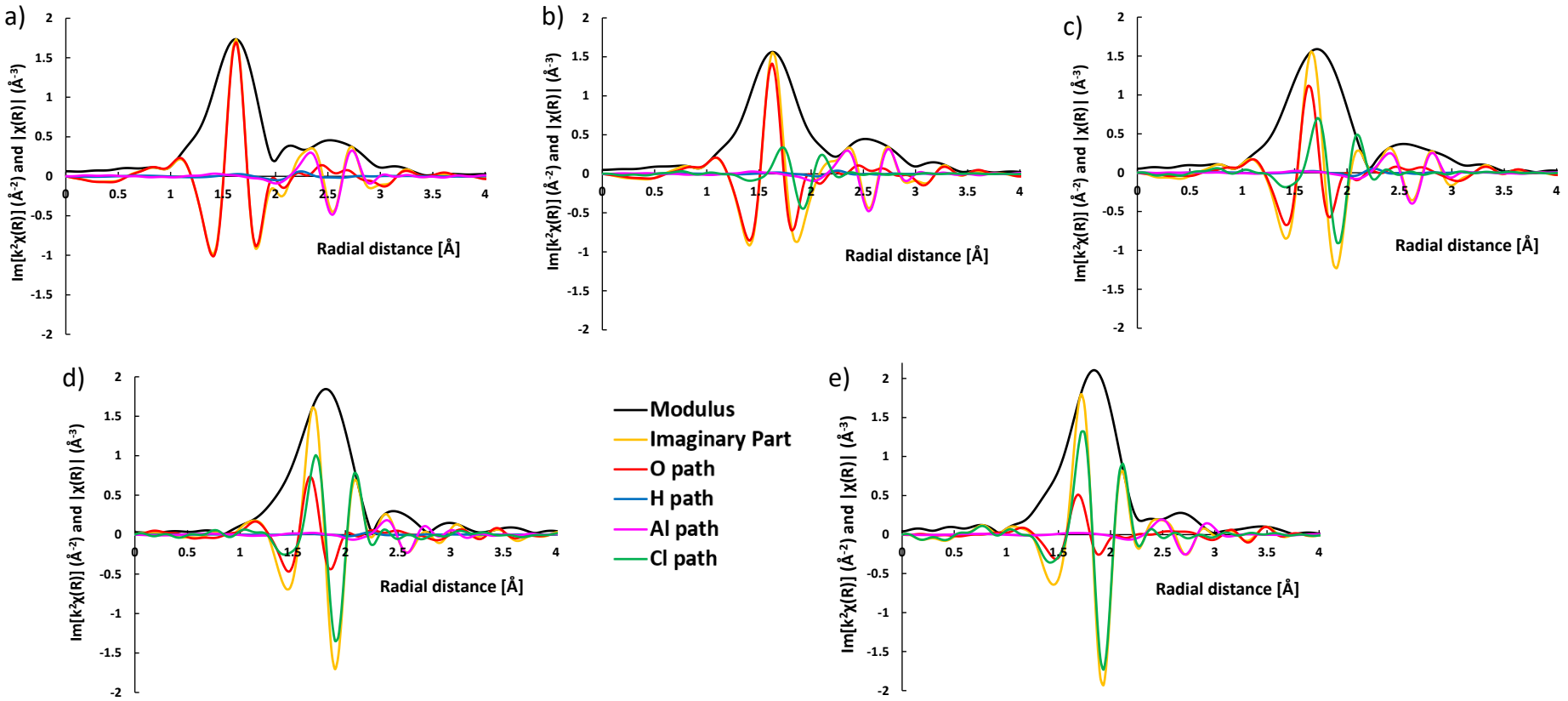

Figure S12. FEFF simulations of the k² weighted Fourier transform modulus and imaginary part associated to the various neighbors paths on the DFT models: a) $Pt(OH)_4H_2O$, b) $Pt(OH)_3Cl(H_2O)$, c) $Pt(OH)_2Cl_2(H_2O)$, d) $Pt(OH)_2Cl_3H$*, e) $PtCl_4(OH)H$*.

SI 12. Details on the XANES analysis of $PtCl_y(OH)_{4-y}(H_2O)$ and $PtCl_y(OH)_{4-y}$ models

Species	While Line peak (eV)
Reference 0.1wt.% Cl	11568.60
Reference 1.4 wt.%Cl	11568.60
$PtCl_4(OH)H^*$	11568.52
$PtCl_3(OH)_2H^*$	11568.96
$PtCl_2(OH)_2(H_2O)$	11569.57
$PtCl(OH)_3(H_2O)$	11570.35
$Pt(OH)_4(H_2O)$	11571.10

Table S4. Measured and computed energies of the whitelines of Pt L_3-edge XANES.

Energy range	0.1 wt.%Cl reference	1.4 wt.%Cl reference
Full	17% $PtCl_2(OH)_2(H_2O)$ 31% $PtCl_3(OH)_2H^*$ 52% $PtCl_4(OH)H^*$	9% $PtCl_2(OH)_2(H_2O)$ 13% $PtCl_3(OH)_2H^*$ 78% $PtCl_4(OH)H^*$
11575-11640	39% $PtCl_2(OH)_2(H_2O)$ 32% $PtCl_3(OH)_2H^*$ 29% $PtCl_4(H_2O)$	1% $PtCl_3(OH)_2H^*$ 99% $PtCl_4(OH)H^*$
11575-11585	27% $PtCl_2(OH)_2(H_2O)$ 73% $PtCl_3(OH)_2H^*$	10% $PtCl_3(OH)_2H^*$ 90% $PtCl_4(OH)H^*$

Table S5. Contributions of the individual computed spectra in the fit of the two experimental spectra. Three ranges of energies are used to produce three different fitted spectra.

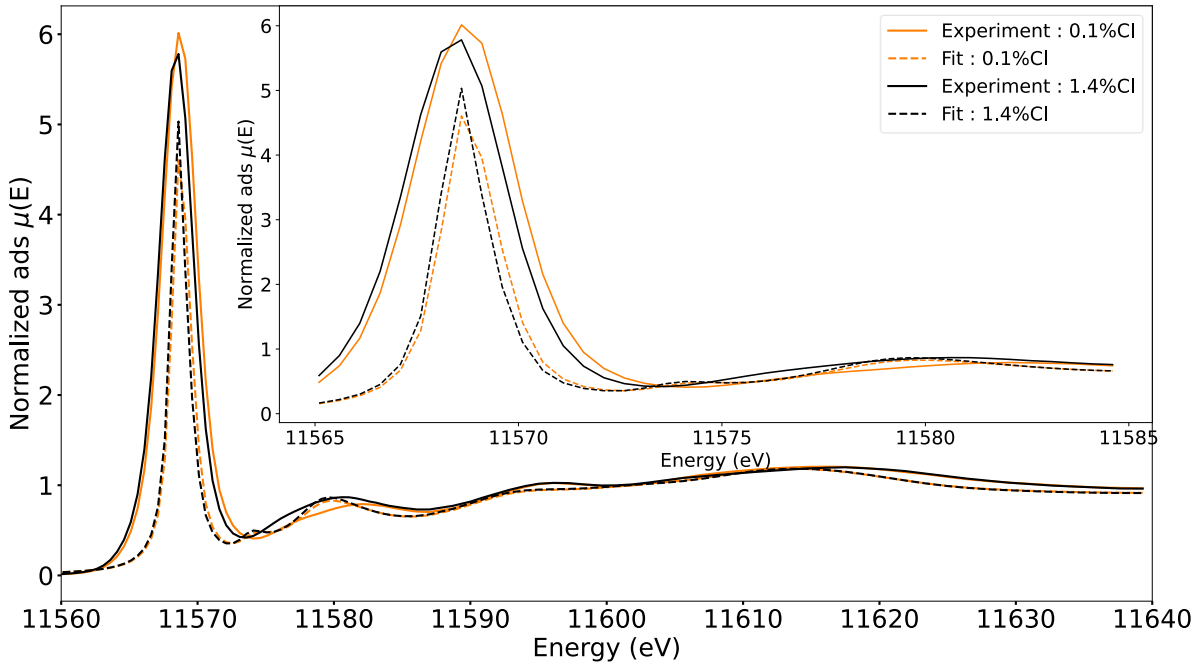

Figure S13. Pt L_3-edge XANES fitted spectra obtained from the $PtCl_y(OH)_{4-y}(H_2O)$. References are the calcinated catalysts obtained for 0.1 wt.% Cl loading (brown) and 1.4 wt.% Cl loading (black). The full range of energies was used to fit the spectra. Composition of the fitted spectra are given in Table S5.

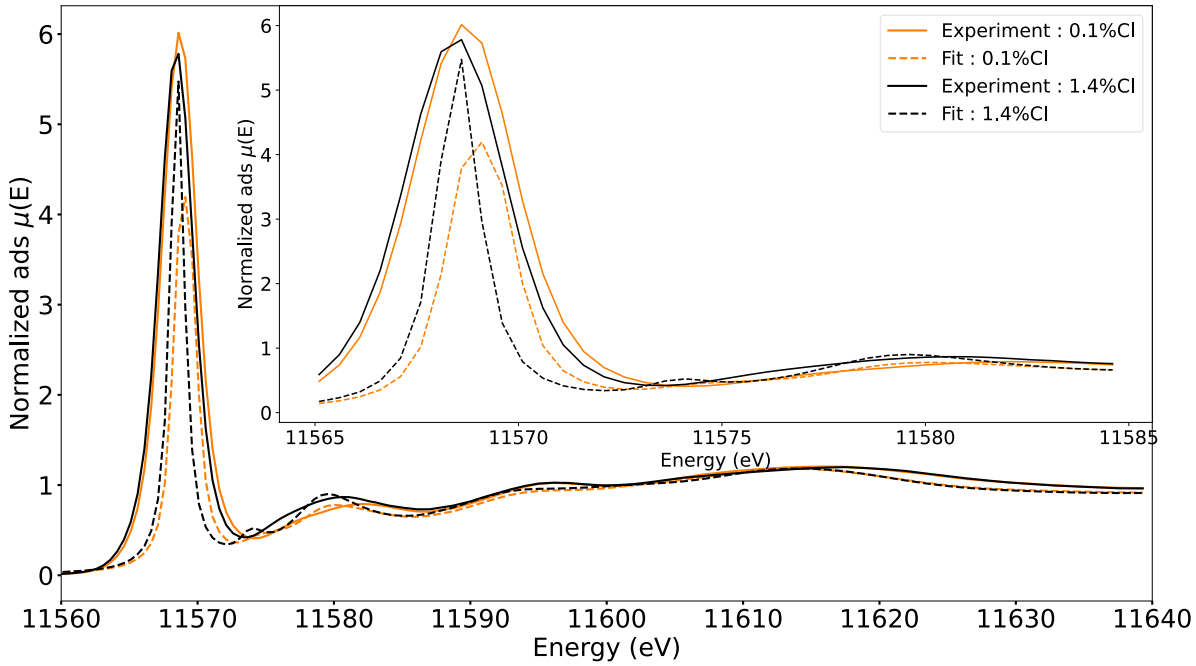

Figure S14. Pt L_3-edge XANES fitted spectra obtained from the $PtCl_y(OH)_{4-y}(H_2O)$. References are the calcinated catalysts obtained for 0.1 wt.% Cl loading (brown) and 1.4 wt.% Cl loading (black). Only energies superior to 11575 eV were used to fit the spectra, excluding the WL. Compositions of the fitted spectra are given in Table S5.

Through the fit over the full range of energies (**Figure S13**), we estimate that the 0.1 wt.% Cl loading reference is composed of 17% of $PtCl_2(OH)_2(H_2O)$, 31% of $PtCl_3(OH)_2H^*$ and 52% of $PtCl_4(OH)H^*$, while the composition of the spectra become 10% of $PtCl_2(OH)_2(H_2O)$, 13% of $PtCl_3(OH)_2H^*$ with 78% of $PtCl_4(OH)H^*$ for the 1.4 wt.% Cl loading catalysts. Despite not being in perfect agreement with EXAFS values, the increase of the quantity of Cl is well reproduced going from an average of 3.3 Pt-Cl for the 0.1 wt.%Cl reference to 3.7 Pt-Cl for the 1.4 wt.%Cl catalyst. Compared to the fit reported in the main text in **Figure 10**, the intensity of the WL is slightly worse.

By avoiding the WL area and starting the fit at 11575 eV (**Figure S144**), another composition is expected with an average of 2.9 Pt-Cl for the 0.1 wt.% Cl reference and 4 Pt-Cl for the 1.4 wt.% Cl. While less chlorinated platinum complexes are now calculated to be in the fit of the low chlorine reference with 39% of $PtCl_2(OH)_2(H_2O)$ and only 29% of $PtCl_4(OH)H^*$, only $PtCl_4(OH)^*H$ is expected in the description of the highly chlorinated spectra.

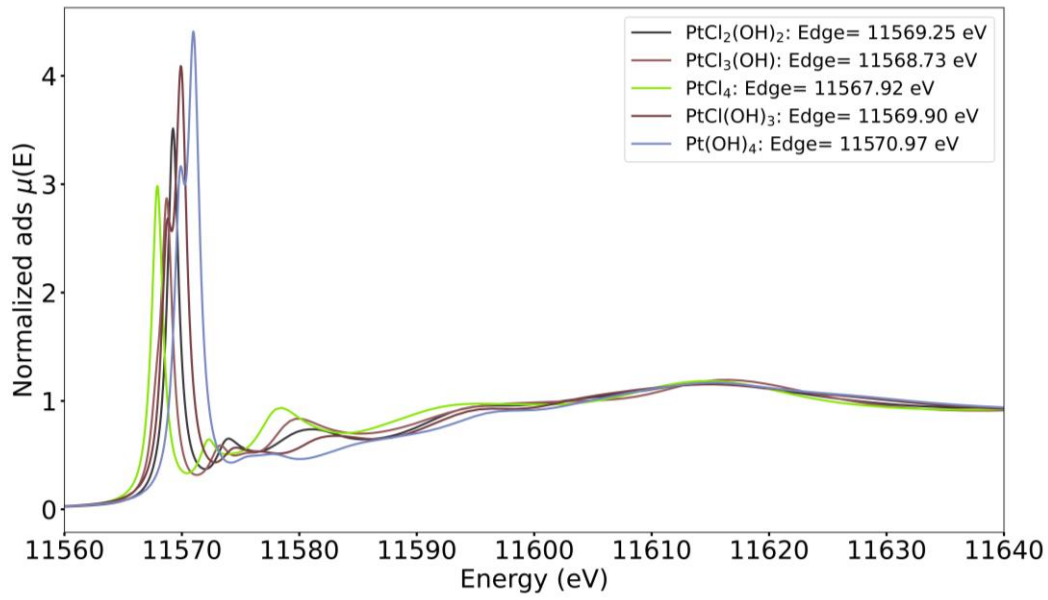

Figure S15. FDMNES simulation of Pt L_3-edge XANES spectra for various relevant non-octahedral $PtCl_y(OH)_{4-y}$ complexes.

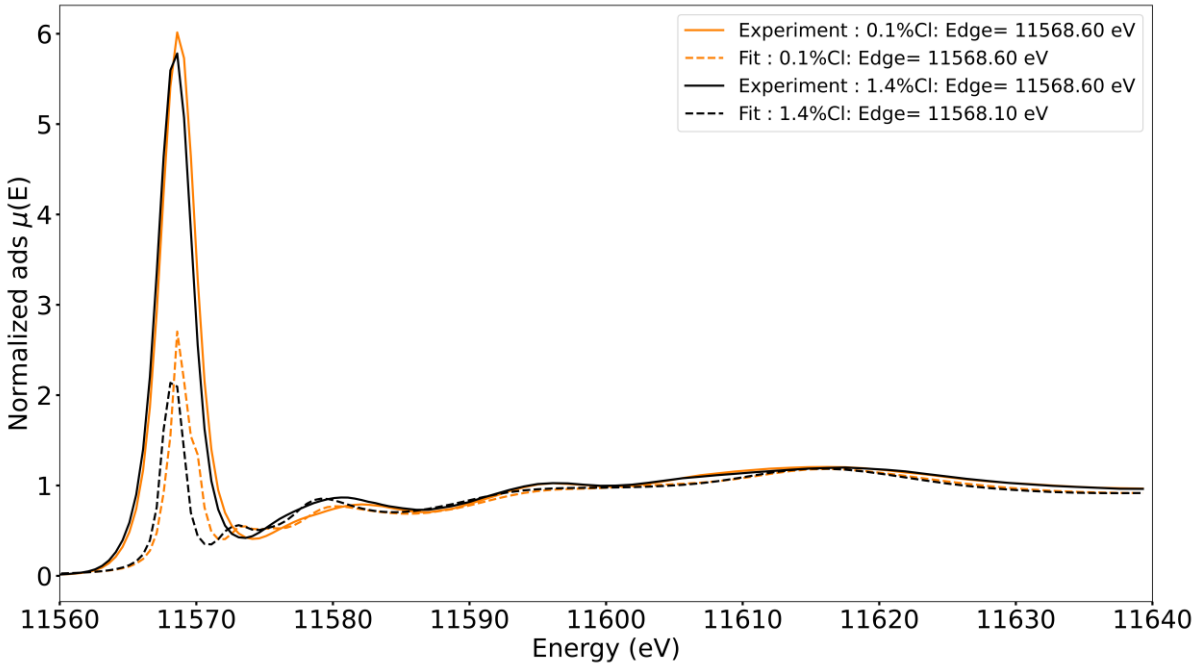

Figure S16. Pt L_3-edge XANES fitted spectra obtained from the non-octahedral $PtCl_y(OH)_{4-y}$. References are the calcinated catalysts obtained for 0.1 wt.% Cl loading (brown) and 1.4 wt.% Cl loading (black). The fit was done for energies between 11575 eV and 11585 eV.

References

[1] M. Digne, P. Sautet, P. Raybaud, P. Euzen, H. Toulhoat, Hydroxyl Groups on γ-Alumina Surfaces: A DFT Study, J. Catal. 211 (2002) 1–5.

[2] A. Hellier, C. Chizallet, P. Raybaud, $PtO_xCl_y(OH)_z(H_2O)_n$ Complexes under Oxidative and Reductive Conditions: Impact of the Level of Theory on Thermodynamic Stabilities, ChemPhysChem (2023) 24, e202200711.